Effective Initial Crack Depth in Exposed Concrete Surfaces

Matthew A. Beyer[1]
Jeffery R. Roesler[2]

Abstract
Microcracking at the surface of concrete slabs can result in a reduction in slab strength at the surface and a decrease in the flexural load carrying capacity of the slab especially when undergoing loading that produces top tensile stresses. The majority of this surface cracking is the result of drying shrinkage gradients and slab restraint. The use of an effective initial crack depth (a_e) has been previously proposed as a method to model this reduction in slab strength due to surface microcracking. The two-parameter fracture model procedure was modified to make calculations of the effective initial crack depth in three-point bending specimens to examine if reasonable values of a_e can be measured in a laboratory setting using fracture mechanics principles. Testing of concrete beams exposed to two curing environments (moist- and dry-cured) indicates that the effective initial crack depth, approximately 50 mm in this study, can be calculated using a dependent relationship between crack depth and compliance values. The procedure was verified by calculating additional fracture parameters of the concrete, which were found to be comparable to values presented in the literature for similar concrete materials and mixtures. The ability to quantify an effective notch depth at the surface of the slab can enable future modeling to determine the effective strength difference of concrete slabs under bottom or top tensile loading conditions.

Introduction

Microcracking at the surface of concrete slabs can result in a reduction in slab strength at the surface and a decrease in the overall load carrying capacity of the slab. McCullough and Dossey (1999) and Rao (2005) observed that the strength of concrete at the top of the slab can be less than the strength at the bottom of the slab due to moisture loss (higher evaporation rates). This early-age surface microcracking has also been shown to be a contributing factor to top-down cracking (Heath and Roesler 2000). The majority of this cracking is the result of shrinkage stresses caused by drying shrinkage gradients and slab restraint. Grasley (2003) found that these high shrinkage gradients exceed the concrete's tensile strength and result in propagation of cracks to some shallow depth from the surface. While restrained shrinkage cracking has been studied in bridge decks, the effects of this microcracking are not currently considered in concrete pavement design (Rao 2005).

---

[1] Member ISCP, Graduate Research Assistant, University of Illinois at Urbana-Champaign, Department of Civil and Environmental Engineering, B233 Newmark Civil Engineering Laboratory, MC-250, 205 North Mathews Ave., Urbana, IL 61801, USA. Email: mabeyer2@uiuc.edu
[2] Member ISCP, Associate Professor, University of Illinois at Urbana-Champaign, Department of Civil and Environmental Engineering, 1211 Newmark Civil Engineering Laboratory, MC-250, 205 North Mathews Ave., Urbana, IL 61801, USA. Email: jroesler@uiuc.edu

Drying shrinkage represents the strain caused by the loss of water from the porous concrete microstructure (Mindess et al. 2003). At early ages, drying shrinkage can be induced by external drying through evaporation, which causes a reduction in the disjoining pressure and an increase in capillary stresses within the concrete (Grasley 2003). Shrinkage stresses at the surface of a slab are not caused by free shrinkage strains but are the result of concrete restrained from making volumetric changes. Types of slab restraint include load transfer and friction with adjacent slabs, friction at the slab-base interface, self-restraint or differential restraint, and the slab's self weight. When these surface stresses exceed the tensile strength of the concrete, microcracking can occur at the slab surface. Typically this cracking does not propagate very far into the slab due to the highly nonlinear stress profile (Rodden et al. 2007) and thus does not typically present itself as a macrocrack.

One approach to characterizing the existence of microcracking at the surface would be to analyze concrete pavement with two different flexural strengths when conducting a fatigue design of the slab: a concrete strength for the bottom of the slab and a reduced concrete strength for the top. An alternative approach is to use an effective initial crack depth (a_e) proposed by Rao (2005) to distinctly model the reduction in slab strength due to surface microcracking. Slabs are still assumed to behave as slabs but with an initial discrete surface crack depth, a_e. The depth of this surface crack is not the depth of a real observable crack at the slab surface but an effective depth that gives the same fracture response. A slab with a small amount of surface microcracking has a lower effective initial crack depth than a slab with a larger amount of surface microcracking. Rao (2005) was able to show that the use of an effective initial crack depth could explain the high variability in the performance among individual concrete slabs that underwent accelerated pavement testing.

The objective of this study is to examine the application of nonlinear elastic fracture mechanics to the study of surface microcracking in laboratory specimens. The two-parameter fracture model (Jenq and Shah 1985) and three-point bending beam specimens with surface microcracking are used to examine if reasonable calculations of effective initial crack depth can be made in a laboratory setting using fracture mechanics principles. While there are limitations to using laboratory beam specimens to explain slab behavior, this proposed method for calculating an effective initial crack depth should serve as a means to begin quantifying the phenomenon of surface microcracking in concrete pavements, which can be subsequently used to model propagation of top-down cracking in thermo-mechanically loaded slabs.

Concrete Mix Design

A concrete mixture with high shrinkage characteristics was designed to ensure that surface microcracking occurred in specimens when exposed to a drying gradient. These types of mixtures are susceptible to shrinkage cracking if adequate moisture curing is not provided at early ages. Because drying shrinkage is directly related to the paste content of concrete, a relatively high water/cement ratio (w/c ratio = 0.50) was used for this mixture, which is summarized in Table 1.

Table 1. Concrete mixture design.

Material	Quantity	
	(lb/cy)	(kg/m^3)
Water	325.0	192.8
Cement	650.0	385.6
Fine Aggregate (SSD)	1132.7	672.0
Coarse Aggregate (SSD)	1739.7	1032.1
w/c ratio	0.50	

The materials used included Type I/II Portland cement, crushed limestone aggregate with a maximum size of 25 mm (1 in.), and natural sand. Measurements of fresh and hardened properties were made and are summarized in Table 2.

Table 2. Average fresh and hardened concrete properties.

Property	Quantity
Fresh concrete	
Slump	233 mm (9.0 in)
Unit Weight	2,400 kg/m^3 (149.8 lb/ft^3)
Air Content	0.6%
Hardened concrete	
Compressive Strength (7-day)	32.0 MPa (4,645 psi)

Specimen Preparation

Four concrete specimens were cast for the first round of three-point bending tests. Six additional beams were later cast for additional testing. The dimensions of the beams are shown in Figure 1. Two different curing methods were used to produce two different effective initial crack depths. Five beams were demolded and placed in a room temperature, moist curing chamber 24 hours after initial casting. Because the moist curing chamber had a humidity of 100 percent, moisture was continuously supplied to the concrete, preventing moisture loss and drying shrinkage gradients from developing. For the moist-cured beams, the effective initial crack depth is assumed to be zero (a_e = 0). The five remaining beams were cured in a constant temperature chamber with 50 percent relative humidity 24 hours after initial casting. This environment ensured shrinkage gradients would develop through external drying and evaporation. Microcracking could then occur as the result of self-restraint of the beam (Grasley 2003). Special care was taken to ensure that microcracking occurred on the surface of the dry-cured beams. Five out of six of the beam faces were covered with aluminum foil tape, exposing only the top surface of the beams to the drying gradient. Figure 2 shows the two different chambers used to cure the beam specimens.

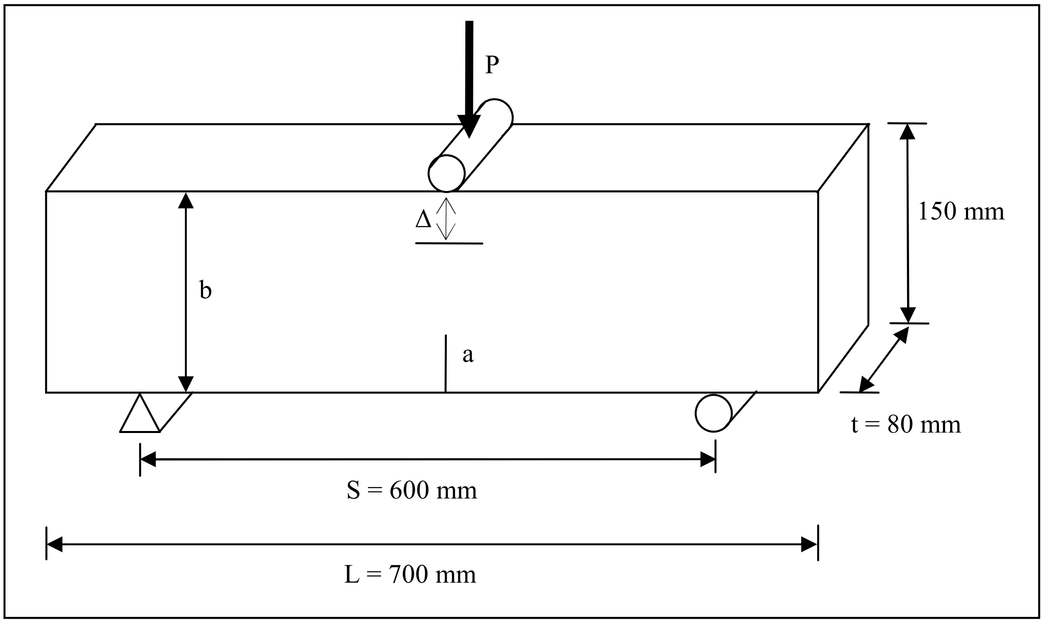

Figure 1. Three-point bending test specimen and load configuration.


Moist Curing *Dry Curing*

Figure 2. Moist and dry curing chambers.

Three-Point Bending Test
The three-point bending test configuration was used to calculate the effective initial crack depth of the surface microcracking in the dry-cured beams. The load configuration of the specimen is shown in Figure 1. The span of the specimen was supported on one end with a roller and on the other with a fixed support. For the dry-cured beams, the load was applied to the surface without microcracking.

Measurements of vertical deflection (Δ) were made at the top surface of the beam using a linear variable differential transformer (LVDT) with an accuracy of 0.1 percent. The test was performed at an initial loading rate of 0.003 mm/min which was controlled by the external LVDT. The applied load (*P*) and specimen deflection (Δ) data were collected at a frequency of 10 Hz. Each beam was monotonically loaded to its peak value and unloaded to zero after 95% of the peak load had been reached. Cyclic loading and unloading continued until fracture of the beam occurred.

Loading and unloading cycles were used in accordance with the two-parameter fracture model (TPFM) developed by Jenq and Shah (1985). This procedure uses the elastic fracture response of structures to determine the effective elastic crack length and other fracture parameters (Shah et al. 1995). The TPFM typically uses measurements of crack mouth opening displacement (*CMOD*) and load (*P*) to calculate loading and unloading compliances. Because no measurable crack openings existed for the beams tested, including those with surface microcracking, compliance was instead calculated as the inverse slope of the load (*P*) versus vertical displacement (Δ) curves obtained from the loading and unloading cycles. For each cycle, the loading compliance (C_i^*) is calculated as the inverse slope of the load versus vertical displacement loading curve from 30 to 60 percent of the peak load. The unloading compliance (C_u^*) is calculated as the inverse slope of the load versus vertical displacement unloading curves from 70 to 10 percent of the peak load. Figure 3 shows the loading and unloading compliances for the first cycle of a moist-cured beam.

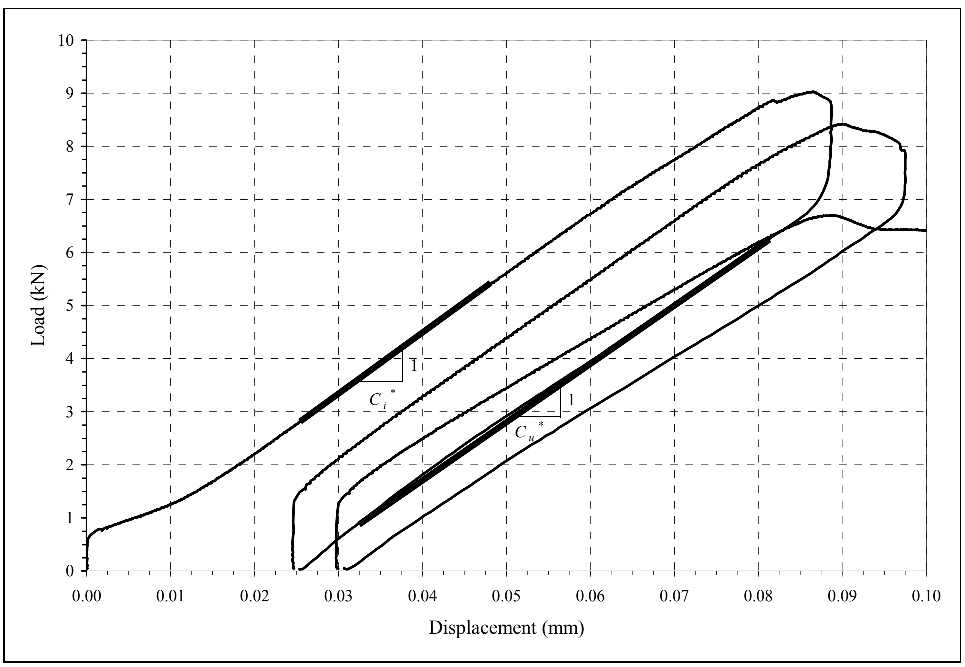

Figure 3. Load (*P*) versus vertical displacement (Δ) for two loading-unloading cycles of a moist-cured beam showing the initial loading (C_i^*) and unloading (C_u^*) compliances.

Testing of the beams was carried out at an age of 16 days. Due to the development of this new test protocol, the results of five of the beams were excluded from further analysis due to inconsistencies in the load versus vertical deflection measurements. Consequently, calculations of loading and unloading compliance were made for three moist-cured beams and two dry-cured beams. Figures 4 and 5 present the loading and unloading curves for the first five cycles of a moist-cured and a dry-cured beam, respectively.

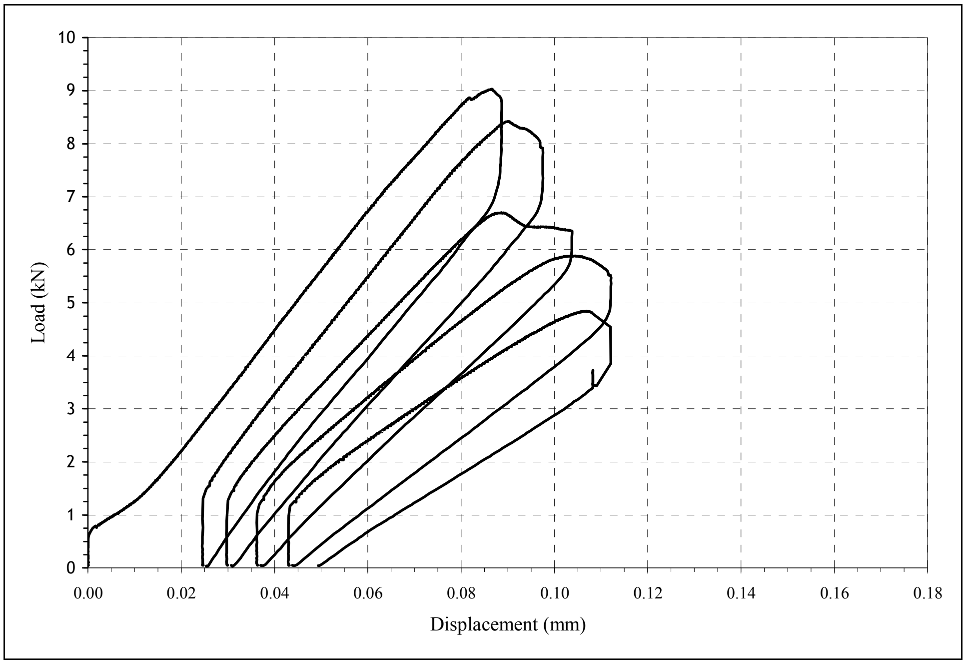

Figure 4. Load (P) versus vertical displacement (Δ) for five loading-unloading cycles of a moist-cured beam.

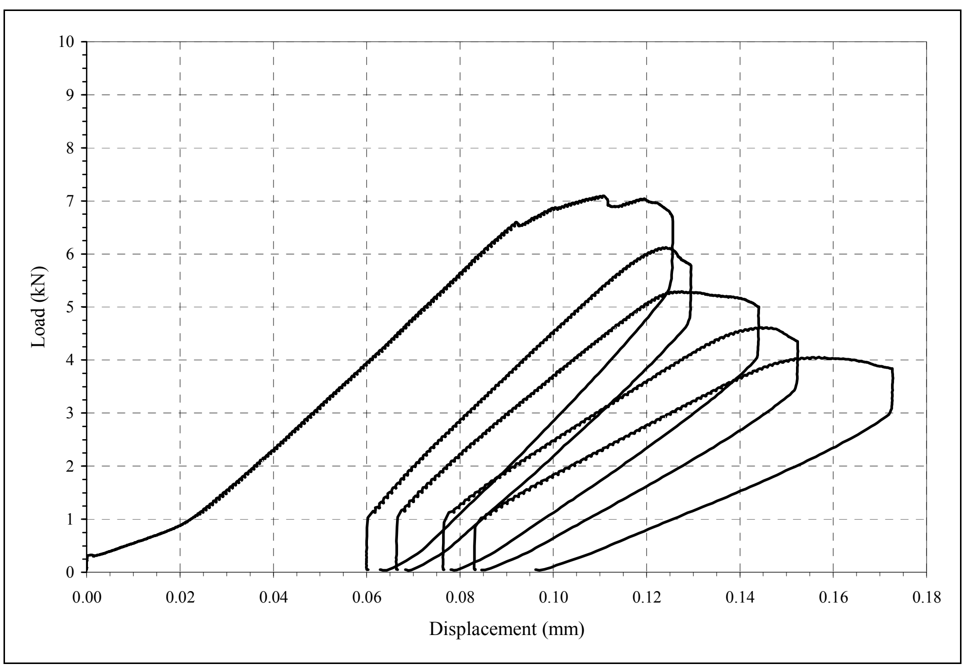

Figure 5. Load (P) versus vertical displacement (Δ) for five loading-unloading cycles of a dry-cured beam.

Fracture Mechanics Calculations

Theoretical Calculations. The effective initial crack depth can be calculated by equating the loading and unloading compliances with the elastic moduli calculated from each cycle. Two key assumptions are made as part of this procedure. The first assumption is that the effective initial crack depth for the moist-cured beam is assumed to be equal to zero ($a_e = 0$). The second assumption is that the method of curing does not affect the elastic modulus of the concrete. The moist- and dry-cured beams are assumed to have approximately the same elastic modulus.

For any load-unload cycle, two crack depths exist: the initial crack depth (a_0) and the critical crack depth (a_c). The initial crack depth is the crack depth at the start of the loading cycle. The critical crack depth is the crack depth at the end of the loading cycle and the start of the unloading cycle. The relationship between a_0 and a_c is given as:

$$a_c = a_0 + \Delta a \tag{1}$$

where Δa is the amount of crack propagation in the particular load-unload cycle. The effective initial crack depth (a_e) of the beam is equal to the initial crack depth for the first cycle. The crack depth ratio is calculated from the crack depth (a) and the depth of the beam (b = 150 mm) as:

$$\alpha = \frac{a}{b} \ . \tag{2}$$

The next step is to calculate the concrete's elastic modulus. The load point displacement of a beam in three-point bending can be calculated as the sum of two components: one due to load alone and another due to the presence of a crack:

$$\Delta_{TOTAL} = \Delta_{NO\_CRACK} + \Delta_{CRACK} \ . \tag{3}$$

The displacement due to only the load is calculated from beam theory as:

$$\Delta_{NO\_CRACK} = \frac{PS^3}{48EI} \tag{4}$$

$$I = \frac{1}{12} tb^3 \tag{5}$$

where P is the applied load, S is the span of the beam, t is the thickness of the beam, b is the depth of the beam, and E is the modulus of elasticity of the concrete. Although beam theory calls for measurement of deflection at the neutral axis, displacement was measured at the top surface of the beam with the assumption that the beam is rigid enough to act in the linear elastic range for small deflections. The additional load point displacement at the top surface of the beam due to the presence of a crack is given by Tada (1985) as:

$$\Delta_{CRACK} = \frac{3PS^2}{2Eb^2t} g_2(\alpha) \tag{6}$$

$$g_2(\alpha) = \left(\frac{\alpha}{1-\alpha}\right)^2 \left\{5.58 - 19.57\alpha + 36.82\alpha^2 - 34.94\alpha^3 + 12.77\alpha^4\right\} \tag{7}$$

where $g_2(\alpha)$ is a geometric correction factor for a beam in three-point bending with $S/L = 4$. Using equations 4 through 7, equation 3 can be rewritten in terms of the crack depth ratio and elastic modulus as:

$$\Delta_{TOTAL} = \frac{P}{E}\left[\frac{S^3}{4b^3t} + \frac{3S^2}{2b^2t} g_2(\alpha)\right]. \tag{8}$$

In order to calculate crack depth, the flexural stiffness values calculated from the loading (E_i^*) and unloading (E_u^*) cycles can be derived by rearranging equation 8 as:

$$E_i^* = \frac{1}{C_i^*}\left[\frac{S^3}{4b^3t} + \frac{3S^2}{2b^2t} g_2(\alpha_0)\right] \tag{9}$$

$$E_u^* = \frac{1}{C_u^*}\left[\frac{S^3}{4b^3t} + \frac{3S^2}{2b^2t} g_2(\alpha_c)\right] \tag{10}$$

where C_i^* is the loading compliance, C_u^* is the unloading compliance, α_0 is the initial crack depth ratio ($\alpha_0 = a_0/b$), and α_c is the critical crack depth ratio ($\alpha_c = a_c/b$). Assuming that the local modulus of elasticity of the concrete does not change as the beam is loaded and unloaded, equations 9 and 10 can be set equal to one another:

$$E_i^* = E_u^* = E\,. \tag{11}$$

The stiffness of the concrete in bending is calculated using equation 9 and the loading compliance from the first loading cycle of the moist-cured beam ($a_0 = 0$).

Crack Length Determination. Using the stiffness of the concrete (E), equations 9 and 10 can be iteratively solved to determine crack depth values (a_0 and a_c) for the dry-cured beam and additional loading cycles of the moist-cured beam.

Two different procedures were identified to determine crack depth values. The first procedure uses equations 9 and 10 separately and assumes that the relationships between a_0 and C_i^* is independent of the relationship between a_c and C_u^*. The second procedure sets equations 9 and 10 equal to one another to derive the following dependent relationship between a_0, a_c, C_i^*, and C_u^*:

$$g_2(\alpha_c) = \frac{C_u^*}{C_i^*}\left[\left(\frac{S}{6b}\right) + g_2(\alpha_0)\right] - \frac{S}{6b}. \tag{12}$$

The dependent relationship in equation 12 assumes that the critical crack depth (a_c) of one cycle is equal to the initial crack depth (a_0) of the next cycle. Table 3 shows the calculated crack depth values for the independent procedure, while Table 4 shows the crack depth values determined from the dependent relationship of equation 12. Note that for a given beam specimen, both procedures calculate the same effective initial crack depth. The results of these calculations indicate an average effective initial crack depth (a_e) of 47.6 mm for the beams with exposed surface to drying. Based on theoretical work presented by Rao (2005), an effective initial crack depth equal to one-third of the specimen depth could reduce the nominal strength of the concrete by 50 percent and thus make top-down cracking more likely than previously expected.

Table 3. Crack depth values calculated from the independent procedure.

Specimen	Cycle	Initial Crack Depth (a_0) (mm)	Critical Crack Depth (a_c) (mm)	Δa (mm)
Dry-cured #1	1	37.4*	28.8	-8.7
	2	32.4	37.3	4.9
	3	38.8	51.4	12.6
	4	54.2	60.7	6.5
	5	64.3	71.3	7.1
Dry-cured #2	1	57.8*	42.8	-15.1
	2	52.0	51.1	-0.8
	3	59.0	58.5	-0.5
	4	63.4	64.9	1.5
	5	50.0	70.5	20.4

*Denotes effective initial crack depth (a_e)

Table 4. Crack depth values calculated from the dependent procedure.

Specimen	Cycle	Initial Crack Depth (a_0) (mm)	Critical Crack Depth (a_c) (mm)	Δa (mm)
Dry-cured #1	1	37.4*	28.8	-8.7
	2	28.8	33.9	5.2
	3	33.9	47.5	13.6
	4	47.5	54.7	7.2
	5	54.7	62.9	8.2
Dry-cured #2	1	57.8*	42.8	-15.1
	2	42.8	41.8	-1.0
	3	41.8	41.1	-0.7
	4	41.1	43.2	2.1
	5	43.2	46.5	3.3

*Denotes effective initial crack depth (a_e)

Fracture Parameters. Additional fracture parameters were calculated to verify the results of the crack depth analysis. From linear elastic fracture mechanics, the critical stress intensity factor (K_{IC}) can be calculated using the effective elastic crack length as:

$$K_{IC} = 3\left(P_c + 0.5P_0 S / L\right)\frac{S\sqrt{a_c \pi}\, g_1(\alpha_c)}{2b^2 t} \tag{13}$$

$$g_1(\alpha_c) = \frac{1}{\sqrt{\pi}} \cdot \frac{1.99 - \alpha(1-\alpha)\left(2.15 - 3.93\alpha + 2.70\alpha^2\right)}{(1+2\alpha)(1-\alpha)^{3/2}} \tag{14}$$

where P_0 is the self-weight of the beam and $g_1(\alpha)$ is a geometric correction factor for a beam in three-point bending with $S/L = 4$ (Shah et al. 1995). Likewise, the critical crack tip opening ($CTOD_c$) can be calculated as:

$$\begin{aligned} CTOD_c = {} & 6\left(P_c + 0.5P_0 S / L\right)\frac{S a_c g_3(\alpha_c)}{E b^2 t} \\ & \times \left[(1-\beta_0)^2 + (1.081 - 1.149\alpha_c)\left(\beta_0 - \beta_0^2\right)\right]^{1/2} \end{aligned} \tag{15}$$

$$g_3(\alpha_c) = 0.76 - 2.88\alpha_c + 3.87\alpha_c^2 - 2.04\alpha_c^3 + \frac{0.66}{(1-\alpha_c)^2} \tag{16}$$

$$\beta_0 = \frac{a_0}{a_c} \tag{17}$$

where $g_3(\alpha)$ is a geometric correction factor for a beam in three-point bending with $S/L = 4$ (Shah et al. 1995).

Table 5 shows the calculated K_{IC} and $CTOD_c$ values for the first load-unload cycles for both the moist- and dry-cured beams. Critical crack tip opening ($CTOD_c$) values were not obtained for the dry-cured beams because of the negative Δa values shown in Tables 3 and 4. While Tables 5 shows some variability in the fracture parameters between specimens, the average K_{IC} and $CTOD_c$ values are comparable to those of previous fracture studies that used the three-point bending test configuration. Roesler et al. (2007) calculated average K_{IC} and $CTOD_c$ values of 1.13 MPa-m$^{1/2}$ and 0.0180 mm, respectively, for a concrete mixture using Type C fly ash with a water/cement ratio of 0.42.

Table 5. Fracture parameters calculated from the crack depth results.

Type	Specimen	Peak Load (kN)	K_{IC} (MPa-m$^{1/2}$)	$CTOD_c$ (mm)
Moist-cured	1	9.028	0.898	0.0130
	2	7.342	1.014	0.0251
	3	9.209	1.023	0.0164
AVERAGE		8.527	0.978	0.0181
CV (%)		12.1	7.1	34.3
Dry-cured	1	7.098	1.065	—
	2	6.751	1.292	—
AVERAGE		6.924	1.179	—
CV (%)		3.5	13.6	—

Discussion

As previously stated, an effective initial crack depth (a_e) of 47.6 mm was calculated for the dry-cured beam. Of the two procedures to determine crack depth, the dependent method produces values that make more physical sense than the independent method. Table 3 shows that for the independent calculation procedure, the critical crack depth (a_c) of one unloading cycle does not have the same magnitude as the initial crack depth (a_0) of the next loading cycle. Because crack propagation should not occur during the unloading cycle, the two crack depth values should be equal to one another. Recall that the dependent calculation procedure assumes that these two values are identical (see Table 4). As a result, the dependent calculation procedure appears to be the preferred method of calculating the effective initial crack depth of the beam.

Tables 3 and 4 show that negative crack propagation (Δa) values where calculated for several loading-unloading cycles. For these cycles, the unloading compliance (C_u^*) was lower than the loading compliance (C_i^*). Because the two-parameter fracture model assumes that crack propagation only occurs when the unloading compliance is greater than the loading compliance, the calculation procedure produces a negative result. These compliance results are an indication that for the initial loading-unloading cycles, significant traction and aggregate interlock exists within the microcracking region and thus a calculated negative crack extension can occur.

It is assumed that the fracture parameters, such as the critical stress intensity factor (K_{IC}) and critical crack tip opening ($CTOD_c$), are inherent material properties based on the TPFM. Ideally, these values should not change between loading and unloading cycles or between specimens cast from the same mixture. The agreement of the calculated fracture parameters with existing values is an indication that the procedure used to calculate effective initial crack depth produces reasonable results.

Conclusion

Microcracking at the surface of concrete slabs, which can result in a reduction in the surface slab strength, has been modeled by previous researchers using an effective initial crack depth (a_e) approach. A two-parameter fracture modeling procedure was modified to make calculations of effective initial crack depth in three-point bending specimens to examine if reasonable values of a_e can be made in a laboratory setting using fracture mechanics principles. Testing conducted on both moist-cured and dry-cured concrete beams indicates that effective initial crack depth can be calculated using a dependent relationship between crack depth and compliance values. The procedure was verified by calculating additional fracture parameters of the concrete, which were found to be comparable to values calculated for similar concrete mixtures in the literature.

This study serves as a proof-of-concept exercise for calculating effective initial crack depth using the two-parameter fracture model. Because of the small number of specimens tested, additional testing is strongly recommended to confirm the findings of this study. Microcracking is affected by a number of factors, including the age of the concrete, mixture constituents and proportions, and the curing method employed. Future work in microcracking could examine how these factors influence effective initial crack depth and the extent of microcracking in different concrete mixtures.

References

Grasley, Z.C. (2003). “Internal Relative Humidity, Drying Stress Gradients, and Hygrothermal Dilation of Concrete.” *Master’s Thesis*, Department of Civil and Environmental Engineering, University of Illinois, Urbana, IL.

Heath, A.C. and Roesler, J. R. (2000). “Top-Down Cracking of Rigid Pavements Constructed with Fast Setting Hydraulic Cement Concrete.” *Transportation Research Board 1712*, TRB, National Research Council, Washington, D.C., 3-12.

Jenq, Y.S., and Shah, S.P. (1985). “A Two Parameter Fracture Model for Concrete.” *Journal of Engineering Mechanics*, 111(4), 1227-1241.

McCullough, B.F. and Dossey, T. (1999). “Considerations for High-Performance Concrete Paving: Recommendations from 20 Years of Field Experience in Texas.” *Transportation Research Record 1684*, TRB, National Research Council, Washington, D.C., 17-24.

Mindess, S., Young, J.F., and Darwin, D. (2003). *Concrete*, 2nd Ed., Prentice-Hall, Upper Saddle River, NJ.

Rao, S.P. (2005). “Characterizing Effective Built-in Curling and its Effect on Concrete Pavement Cracking.” *Ph.D. Thesis*, Department of Civil and Environmental Engineering, University of Illinois, Urbana, IL.

Rodden, R., Roesler, J. and Lange, D. (2007). “A Micromechanical Approach to Computing Linear and Nonlinear Moisture and Temperature Stresses in Concrete Pavements.” *International Conference: Advanced Characterization of Pavement and Soil Engineering Materials*, 20-22 June 2007, Athens, Greece, 7 pp.

Roesler, J., Paulino, G.H., Park, K., and Gaedicke, C. (2007). “Concrete fracture prediction using bilinear softening.” *Cement & Concrete Composites*, 29, 300-312.

Shah, S.P., Swartz, S.E., and Ouyang, C. (1995). *Fracture Mechanics of Concrete*, Wiley, New York.

Tada, H. (1985). *The Stress Analysis of Cracks Handbook*, Paris Productions & Del Research Corp., St. Louis, MO.